Supporting Information

CH-π "T-Shape" Interaction with Histidine Explains Binding of Aromatic Galactosides to Pseudomonas aeruginosa lectin LecA

Rameshwar U. Kadam[a†‡], Divita Garg[b†‡], Julian Schwartz,[a] Ricardo Visini[a], Michael Sattler[b], Achim Stocker[a], Tamis Darbre[a], and Jean-Louis Reymond[a]*

[a]*Department of Chemistry and Biochemistry, University of Berne, Freiestrasse 3, 3012 Berne Switzerland; jean-louis.reymond@ioc.unibe.ch* [b]*Institute of Structural Biology, Helmholtz Zentrum München and Center for integrated Protein Science Munich at Dept Chemie, Technische Universität München, Lichtenbergstr. 4, 85747 Garching, Germany*

Table of Contents

Analysis of His-aromatic contacts in pdb

33,091 pdb files were retrieved from the pdb database (www.rcsb.org; July 2013) corresponding to structures with resolution ≤ 2.0 Å. His-aromatic contacts were identified with the condition that the distance between the centroid of the histidine imidazole ring and the centroid of the other aromatic ring (aromatic ring from side-chain or ligand) is less than 5.0 Å. Redundant pairs were identified as those having the same protein name and the same residue numbers. For each pair, two parameters were measured:

1) The angle α between the normal of each plane spanned by an aromatic ring (0 – 90°)
2) The distance d between the centroid of the histidine ring and the normal line of the other aromatic ring

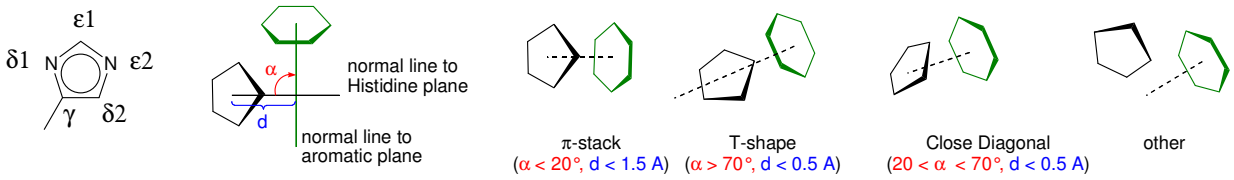

Table S1. Number of His-aromatic contacts found in pdb according to contact type. [a)]

Category	**Sub-cat.**[b)]	**To side chain**[c)] Nr.	%	**Example**	**To ligand**[d)] Nr.	%	**Example**
π-stack[e)]		2263	7.67	Barnase 1RNB[1] HisA18 – TrpA94	189	10.81	Catalase HPII 3P9Q[2] HisB128 – Heme B761
T-shape[f)]	all	634	2.15		23	1.32	
	C(δ2)	340	1.15	Green fluorescent protein 2 2G6Y[3] His181 – His76	12	0.69	Beta-trypsin 1O3E[4] His A57 – CRA_8696 A246
	N(δ1)	69	0.23	Protoglobin 3ZJI[5] HisB121 – TyrB189	1	0.06	Methyl accepting chemotaxis protein 4GLQ[6] HisA523 – Phycoviolobilin A1000
	C(ε1)	**152**	**0.52**	Ferritin-4, chloroplastic 3A68[7] His195A-X – His195A-X	**7**	**0.40**	Tryptophan synthase beta chain 1K8Z[8] HisB86 – pyridoxal phosphate B502
	N(ε2)	70	0.24	Glucose-6-phosphate isomerase 2CVP[9] HisA17 – TyrA331	3	0.17	Insulin 1ZEI[10] HisF5 – *m*-cresol B56
	Cγ	3	0.01		0	0.00	
C. diag.[g)]		487	1.65	Aspartate aminotransferase 7AAT[11] HisA189 – HisA193	17	0.97	Carboxymethylenebutenolidase 1ZJ4[12] HisA202 – *O*-benzylsulfonyl-serine A123
Other		26201	88.8	Cytochrome P450-CAM 1CP4[13] HisA270 – PheA263	1520	87.0	DNA polymerase I 1NKE[14] HisA768 – 2'-deoxycytidine 5'-triphosphate A2
Total		**29585**			**1749**		

[a)] All unique histidine-aromatic residue or histidine-ligand aromatic ring pairs with centroid distance ≤ 5.0 Å are considered. [b)] The T-shape subcategories refer to the His ring atom closest to the centroid of the other aromatic ring (side chain or ligand). [c)] Aromatic residues: Phe, Tyr, Trp, His. [d)] Aromatic rings in ligands were identifed as planar 5-7 membered ring with C, N, O or S allowing ± 10° deviation from planarity. [e)] π-stack: α < 20°, d < 1.5 Å. [f)] T-shape: α > 70°, d < 0.5 Å. [g)] close diagonal: 20° < α < 70°, d < 0.5 Å.

Galactosides

Galactosides used in this study were either purchased from sigma Aldrich (www.sigmaaldrich.com), Carbosynth (www.carbosynth.com/) or Princeton biomolecular research (www.princetonbio.com), or synthesized as reported previously (GalAG0 and GalBG0).

Table S2. List of commerical compounds purchased for this study with their codes and corresponding chemical suppliers.

Ligand	Name	Compound codes	Suppliers
1	D-(+)-Galactose	G0750	Sigma
2	Isopropyl β-D-1-thiogalactopyranoside	I5502	Sigma
4	5-Fluorouridine-5'-O-β-D-galactopyranoside	NF04428	Carbosynth
5	Phenylethyl-β-D-thiogalactopyranoside	EP03215	Carbosynth
6	4-Nitrophenyl β-D-galacto-pyranoside	N1252	Sigma
8	Phenyl β-D-galactopyranoside	MP02392	Carbosynth
9	4-Aminophenyl β-D-galactopyranoside	MA06133	Carbosynth
10	4-Methylphenyl β-D-galactopyranoside	MM04901	Carbosynth
11	Phenyl β-D-thiogalactopyranoside	MP05112	Carbosynth
12	2-Naphthyl β-D-galactopyranoside	860492	Sigma
13	3, 4-Methylumbelliferyl β-D-galactopyranoside	OSSK_936796	Princeton BR.
14	6-methyl-cyclopenta[c]coumarin β-D-galactopyranoside	OSSK_936757	Princeton BR
15	1-Methyl-3-indolyl-β-D-galactopyranoside	67610	Sigma
16	Resorufin β-D-galactopyranoside	R4883	Sigma
17	Chlorophenol Red-β-D-galactopyranoside	59767	Sigma

Thermodynamic profiling- Isothermal Titration Calorimetry (ITC)

ITC studies were performed in 0.1 M Tris-base, pH 7.5, 25 mM $CaCl_2$ at 25 °C on a VP-ITC calorimeter (MicroCal Inc.). The data were fitted with MicroCal Origin 8 software, according to standard procedures using a single-site model. Change in free energy ΔG was calculated from the equation: $\Delta G = \Delta H - T\Delta S$ where T is the absolute temperature, ΔH and ΔS are the change in enthalpy and entropy respectively (Figure S1a&b).

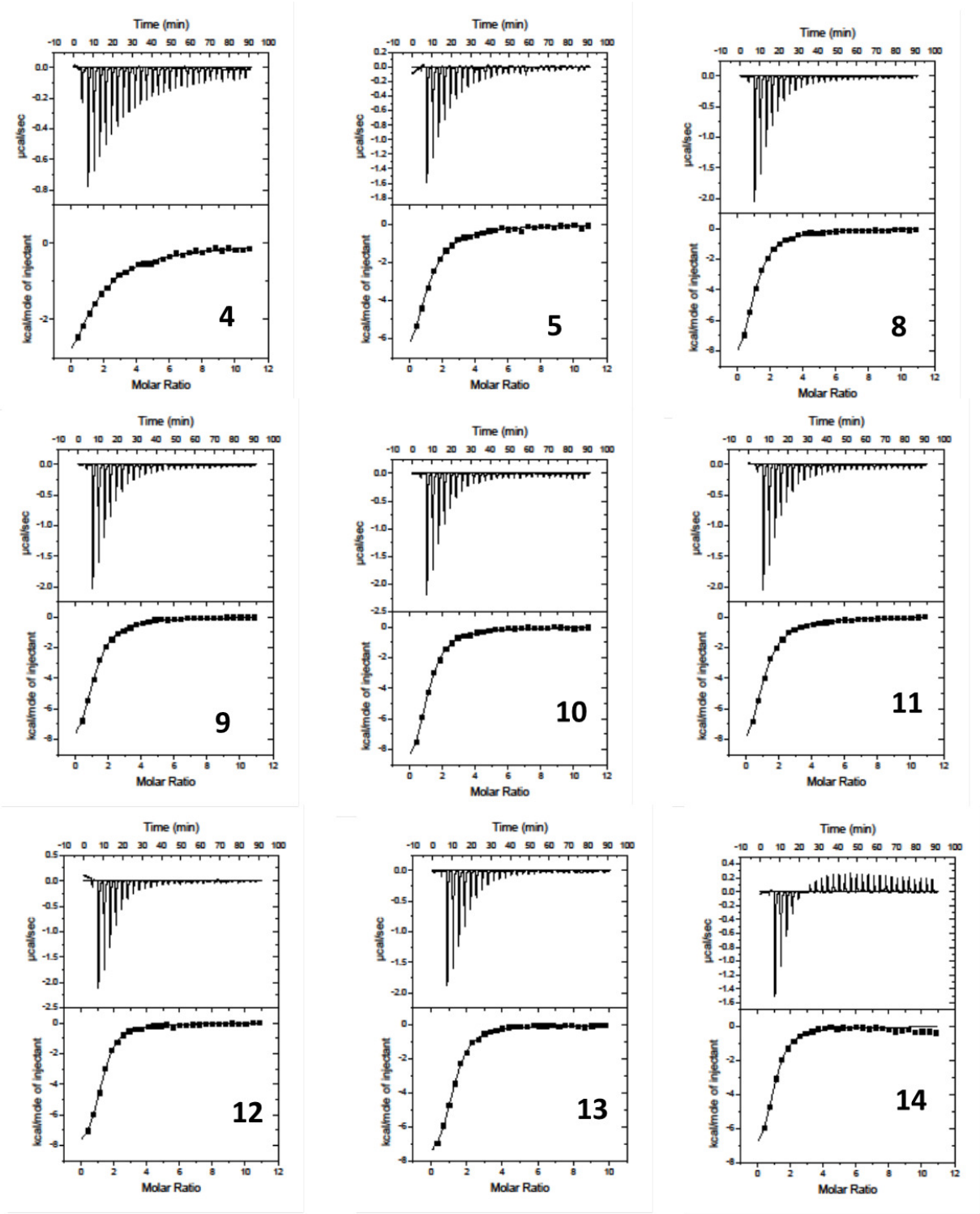

Figure S1a. Isothermal Titration Calorimetric (ITC) measurements representing the raw ITC data (above) and integrated titration curves (below) for the binding of galactosides ligands to LecA. Conc. Of LecA/ligands reported in bracket. Titrant galactosides; **4)** 5-Fluorouridine-5'-O- β -D-galactopyranoside (20 µM /1 mM), **5)** Phenylethyl β-D-thiogalactopyranoside (20 µM /1 mM), **8)** Phenyl β-D-galactopyranoside (20 µM /1 mM), **9)** 4-Aminophenyl β -D-galactopyranoside (20 µM /1 mM), **10)** 4-Methylphenyl β-D-galactopyranoside (20 µM /1 mM), **11)** Phenyl β -D-thiogalactopyranoside (20 µM /1 mM), **12)** 2-Naphthyl-β-D-galactopyranoside (20 µM /1 mM), **13)** 3, 4-Methylumbelliferyl β -D-galactopyranoside (20 µM /1 mM). **14)** 6-methyl-cyclopenta[c]coumarin β-D-galactopyranoside (20 µM /1 mM).

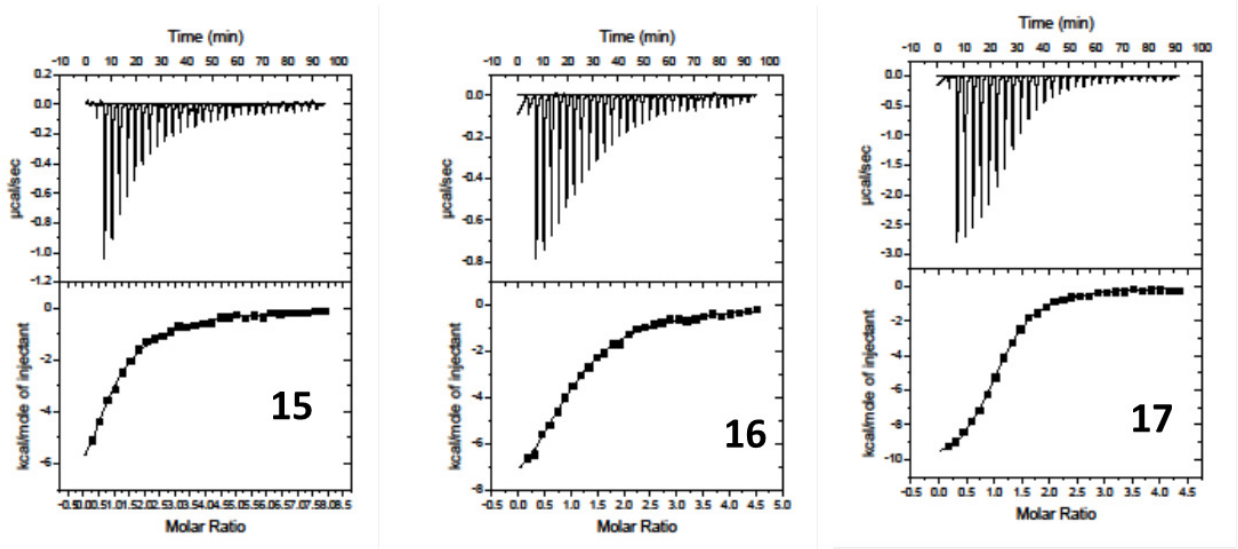

Figure S1b. Isothermal Titration Calorimetric (ITC) measurements representing the raw ITC data (above) and integrated titration curves (below) for the binding of galactosides ligands to LecA. Titrant galactosides; **15)** 1-Methyl-3-indolyl- β-D-galactopyranoside (20 µM /1 mM), **16)** Resorufin -β – galactopyranoside (20 µM /2 mM), **17)** Chlorophenol Red-β-D-galactopyranoside (20 µM /2 mM). The ITC experiments were conducted at c values of 1-5, which generates accurate ΔH and K_D values with known stoichiometry and saturation as was the case here.[15]

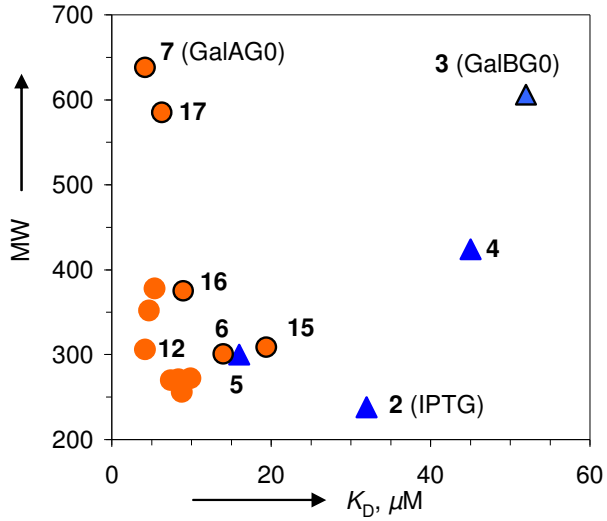

Figure S1c. Scatter plot of LecA affinities versus molecular weight (MW) of aromatic β-galactosides (orange circles) and non-aromatic β-galactosides (blue triangles). Data from Table 1.

Hemagglutination Assay

The rabbit erythrocytes were prepared and lectin titer (HA unit) was determined as per reported protocol.[16] Two fold serial dilutions of 50 µL sample of each inhibitor were prepared in PBS and incubated with 50 µL of LecA solution corresponding to 8 HA units (1.95 µg/mL) for 30 min at 4°C. Subsequently, 50 µL of the erythrocytes were added, mixed and incubated for one hour at the room temperature, followed by centrifugation for 30s at 1,000 g. The highest dilution causing a complete inhibition of hemagglutination (minimal inhibitory concentration MIC) was recorded as the activity of the tested compound. Each test was performed in triplicate.

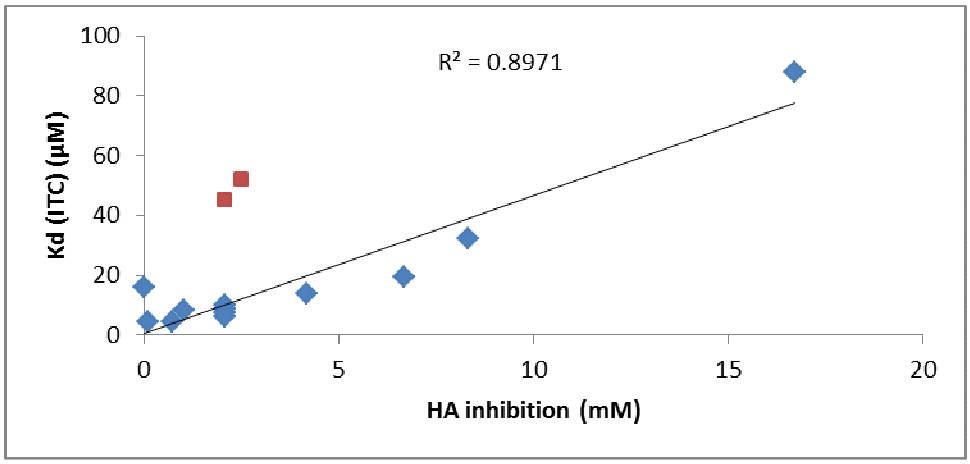

Figure S2. Plot of hemagglutination inhibition MIC vs Kd values from ITC for all compounds in table 1. The correlation coefficient R^2 has been calculated for compounds marked as blue diamonds, whereas the two compounds **GalBG0** (**3**) and **4** (red squares) have been treated as outliers.

P. aeruginosa lectin LecA expression and purification

Escherichia coli BL21(DE3) cells transformed with the plasmid containing the LecA gene pET25paIL were grown in LB medium to OD600nm=0.6 and induced with IPTG at 30 °C. The cells were broken and LecA purified by affinity chromatography along an optimized protocol reported earlier.[16]

X-ray Crystallography of galactosides

Lyophilized LecA was dissolved in water (10 mg/ml) with 1 mM $CaCl_2$ and $MgCl_2$ and the respective galactoside ligand (0.5 mg/ml). Nicely diffracting crystals were obtained for **15**, **16** and **17** in Index I-8 (0.1 M Sodium acetate trihydrate; 3.0 M Sodium chloride, pH 4.5), crystal screen II-9 (0.1 M Sodium acetate trihydrate, 2.0 M sodium chloride, pH 4.6) and Index I-8 (2.4 M Sodium malonate, pH 7.0) (Hampton Research, Laguna Niguel, CA, USA) respectively, using the sitting drop method at 20˚C. Crystals were cryo-cooled at 100 K after briefly soaking them in glycerol 25% v/v in precipitant solution. All data were collected at the SLS synchrotron (Villigen, Switzerland) at beamline PX-III. Data were integrated and scaled with the X-ray detector software for processing single-crystal monochromatic diffraction data (XDS). Details of data collection statistics are reported in Table S2. The structures of the co-crystallized ligands were solved by the molecular replacement technique with the Phaser program, using the monomeric structure (PDB code 3ZYB). The molecular replacements gave clear solutions for all three ligand complexes and the corresponding electron density maps of the complexes showed clear features corresponding to the respective ligand. Automatic placement of water molecules was performed using the ARP/wARP program. Crystallographic refinements were carried out with the program phenix.refine from the PHENIX program package and manual model building with COOT.

Table S3. Data collection and refinement statistics for the **15. LecA, 16.LecA** and **17. LecA**

Structural data	**15. LecA**	**16. LecA**	**17. LecA**
Beam line	PSI PX III	PSI PX III	PSI PX III
Wavelength (Å)	1.00000	1.00000	1.00000
Resolution (Å)	47.40-1.45 (1.53-1.45)*	47.31-1.76 (1.86-1.76)*	48.92-2.86 (3.03-2.86)*
Cell dimension			
Space group	$P2_12_12_1$	$P2_12_12_1$	$P2_12_12_1$
Unit cell (Å)	a = 49.6, b = 68.2, c = 159.4; α = β = γ = 90°	a = 49.5, b = 69.5, c = 158.3; α = β = γ = 90°	a = 89.0, b = 150.0, c = 185.0; α = β = γ = 90°
Measured reflection / unique	609548 / 181878	338308 / 103028	374575 / 109598
Average multiplicity	3.4 (3.3)	3.3 (3.1)	3.4 (3.2)
Completeness (%)	98.1 (93.4)	97.7 (89.4)	97.7 (90.2)
Average I / σ(I)	13.4 (1.91)	11.5 (2.60)	10.48 (2.19)
R_{merge} (%)	16.9 (95.8)	16.3(71.1)	18.5 (72.0)
Wilson B-factor	21.97	25.97	49.21
Refinement			
Resolution range (Å)	47.40-1.45	47.31-1.76	48.92-2.86
R_{work} (%)	18.95	19.47	23.51
R_{free} (%)	21.12	22.27	27.08
Average Biso (Å^2)			
All atoms	22.21	25.56	53.45
Protein atoms	19.72	24.20	30.41
Sugar atoms	21.86	32.07	66.67
Solvent atoms	35.58	33.38	47.01
RMSD from ideality angles (°)	1.00	1.01	0.510
Bonds (Å)	0.005	0.006	0.001
Water molecules	675	548	294
Number of galactose	4	4	12
Calcium atoms	4	4	12
Protein Data Bank deposition code	4LJH	4LK7	4LK6

Note-*Values between parentheses correspond to the highest resolution shell. The following Programs were used in the data processing and refinement- XDS,[17] Phaser, [18] ARP/wARP [19], PHENIX, [20] COOT.[21]

Molecular Modeling of Galactosides

1. Molecular docking and scoring

A. Galactosides ligands geometry optimization.

Galactosides used in this study were the built using maestro interface and subsequently, geometry optimized by Macromodel program v9.1 (Schrodinger, LLC) using the Optimized Potentials for Liquid Simulations-all atom (OPLS-AA) force field[22] with the truncated Newton conjugate gradient protocol. Partial atomic charges were computed using the OPLS-AA force field.

B. Protein structure preparation and refinement

The X-ray crystal structure of lectin LecA from *Pseudomonas aeruginosa* in complex with **6** (PDB ID: 3ZYF) obtained from the RCSB Protein Data Bank (PDB) (http://www.rcsb.org) was used in order to model the protein structure in this study. Water molecules of crystallization were kept 5Å around co-crystalized ligand, and the protein was optimized for docking using the protein preparation and refinement utility provided by Schrödinger LLC. Partial atomic charges were assigned according to the OPLS-AA force field.

C. Docking Methodology and Protocol

All docking calculations were performed using the ‘‘Extra Precision’’ (XP) mode of Glide program[23, 24]. The accuracy of a docking procedure can be evaluated by determining how closely the lowest energy pose (binding conformation) predicted by the object scoring function resembles an experimental binding mode as determined by X-ray crystallography. In the present study, Extra Precision Glide docking procedure was validated by removing the ligand from **6** from the co-crystallized LecA complex and re-docking into the binding site of LecA. A good agreement was observed between the localization of the inhibitor upon docking and from the crystal structure, i.e. having similar hydrogen bonding interactions with Asn107, Asp100, Gln53, His50 and Ca^{2+} co-ordination. The pairwise atom root mean square (RMS) between the predicted conformation and the observed X-ray crystallographic conformation of **6** equaled 0.53 Å (Figure S3), a value that suggests the reliability of the docking program and Glide parameter set in reproducing the experimentally observed binding mode for LecA from *Pseudomonas aeruginosa*. The validated docking protocol was then used for docking galactosides into the crystal structure of the protein.

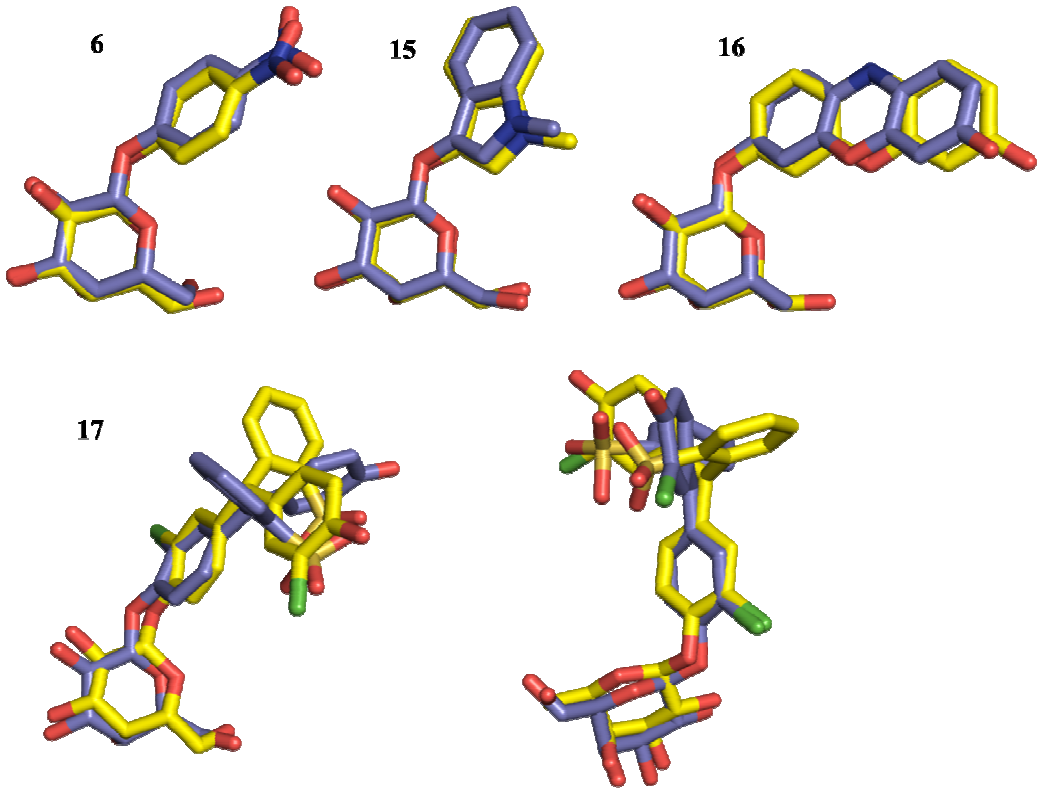

Figure S3 *Overlay of docked vs X-ray conformation*. The pairwise atom RMS values between docked pose (blue) *vs* X-ray crystallographic (yellow) conformation are **6** (0.53Å), **15**(0.53 Å), **16** (0.92 Å), and **17** (3.63 Å). Two different orientations of **17** shown.

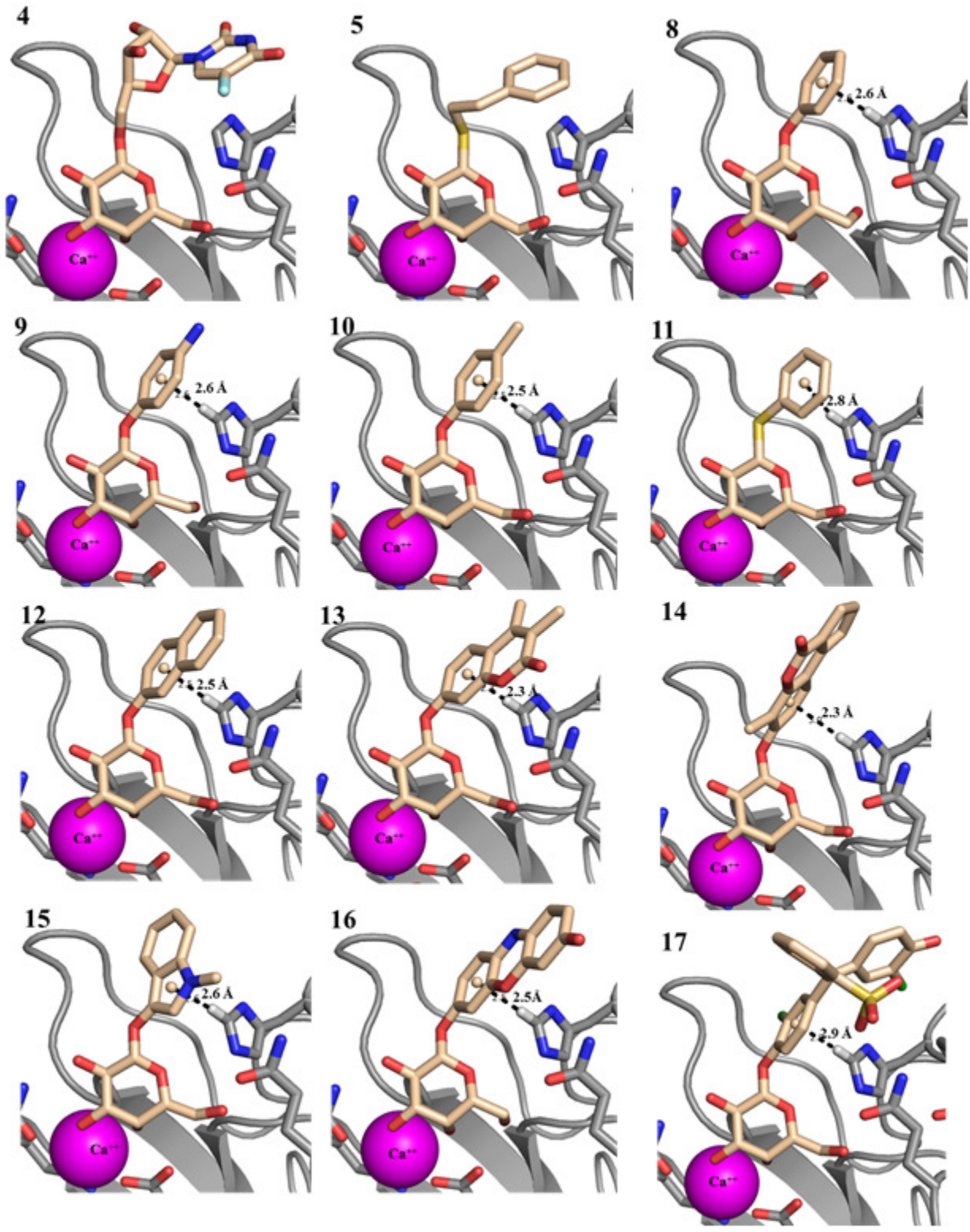

Figure S4: *Predicted binding mode from Molecular docking study*: galactosides used in this study (beige sticks) docked in the LecA binding site. The predicted binding modes support the formation of CH/π T-stack between ligands (**8**-**17**) and C(Ɛ)-H of His50 (LecA); centroids of the T-stacking rings (beige spheres) have been used to estimate the T-stacking distance Predicted binding modes of **4**, **5** do not support the formation of T-stacks. Magenta sphere represents the Ca^{++} ion.

Non Covalent Interactions in aromatic glycoside-protein

Table S4. Non-covalent XH/Cation/π-π interactions in aromatic glycoside-protein complexes.

Protein	PDb code	Stack Type	Residues involved	HpB	Residues involved	H-B	Residues involved	VDW	Binding ratio
OH-π interactions									
Concanavalin A[25, 26]	1VAM 1CJP	OH-π	Tyr^{12}	2	Tyr^{100}, Leu^{99}	1	Tyr^{100}	0	12 x
T. cruzi trans-Sialidase[27]	1S0J	OH-π	Tyr^{119}	1	Trp^{312}	-	-	2	ND
Maclura pomifera agglutinin[28]	3LM1	OH-π	Tyr^{78}	-	-	1	Glu^{76}	1	12 x
CH-π inreactions									
Sialoadhesin[29]	1OD9	CH-π	Val^{109}	1	Leu^{107}	2	Leu^{107}	0	2.1x
Sialoadhesin[29]	1OD7	CH-π	Val^{109}	2	Tyr^{44}, Leu^{107}	2	Leu^{107}	2	11 x
Sialoadhesin[29]	1ODA	CH-π	Val^{109}	2	Tyr^{44}, Leu^{107}	2	Leu^{107}	2	13 x
Lectin from Dioclea violacea	3AX4	CH-π	Leu^{99}	2	Tyr^{12}, Tyr^{100}	1	Tyr^{12}	0	ND
Lectin from Dioclea wilsonii Standl[30]	3SH3	CH-π	Leu^{99}	2	Tyr^{12}, Tyr^{100}	1	Tyr^{12}	0	ND
Human galectin-1[31]	3T2T	CH-π	Val^{31}	-	-	-	-	1	2.5 x
Lysozyme[32]	1BB7	CH-π	Val^{109}	-	-	-	-	3	ND
Cation-π interaction									
Human Galectin-3[31, 33]	3T1L	*Cation-π*	Arg^{144}	-	-	1	Trp^{181}	0	20 x
π-π interaction									
Galactoside Acetyltransferase[34]	1KRV	π-π	Tyr^{83}	-	-	1	Asp^{17}	2	ND
FimH lectin[35]	3MCY	π-π	Tyr^{48}	1	Tyr^{137}	1	Arg^{98}	2	1000 x
Edge-to-Face interaction									
Amaranthus caudatus agglutinin[36]	1JLX	*Edge-to-Face*	Phe^{135}	-	-	-	-	1	2 x

Note- HpB= hydrophobic interactions, H-B= hydrogen bond, VDW= number of Van der Waal interactions in addition to other mentioned contacts. Binding ratio= relative binding of aromatic glycosides compared to natural ligand.

References

1. Baudet, S., and Janin, J. (1991) Crystal structure of a barnase-d(GpC) complex at 1.9 A resolution, *J. Mol. Biol. 219*, 123-132.
2. Jha, V., Louis, S., Chelikani, P., Carpena, X., Donald, L. J., Fita, I., and Loewen, P. C. (2011) Modulation of heme orientation and binding by a single residue in catalase HPII of Escherichia coli, *Biochemistry 50*, 2101-2110.
3. Evdokimov, A. G., Pokross, M. E., Egorov, N. S., Zaraisky, A. G., Yampolsky, I. V., Merzlyak, E. M., Shkoporov, A. N., Sander, I., Lukyanov, K. A., and Chudakov, D. M. (2006) Structural basis for the fast maturation of Arthropoda green fluorescent protein, *EMBO Rep. 7*, 1006-1012.
4. Katz, B. A., Elrod, K., Verner, E., Mackman, R. L., Luong, C., Shrader, W. D., Sendzik, M., Spencer, J. R., Sprengeler, P. A., Kolesnikov, A., Tai, V. W., Hui, H. C., Breitenbucher, J. G., Allen, D., and Janc, J. W. (2003) Elaborate manifold of short hydrogen bond arrays mediating binding of active site-directed serine protease inhibitors, *J. Mol. Biol. 329*, 93-120.
5. Pesce, A., Tilleman, L., Donne, J., Aste, E., Ascenzi, P., Ciaccio, C., Coletta, M., Moens, L., Viappiani, C., Dewilde, S., Bolognesi, M., and Nardini, M. (2013) Structure and Haem-Distal Site Plasticity in Methanosarcina acetivorans Protoglobin, *PLoS One 8*, e66144.
6. Burgie, E. S., Walker, J. M., Phillips, G. N., Jr., and Vierstra, R. D. (2013) A photo-labile thioether linkage to phycoviolobilin provides the foundation for the blue/green photocycles in DXCF-cyanobacteriochromes, *Structure 21*, 88-97.
7. Masuda, T., Goto, F., Yoshihara, T., and Mikami, B. (2010) Crystal structure of plant ferritin reveals a novel metal binding site that functions as a transit site for metal transfer in ferritin, *J. Biol. Chem. 285*, 4049-4059.
8. Weyand, M., Schlichting, I., Herde, P., Marabotti, A., and Mozzarelli, A. (2002) Crystal structure of the beta Ser178--> Pro mutant of tryptophan synthase. A "knock-out" allosteric enzyme, *J. Biol. Chem. 277*, 10653-10660.
9. Tanaka, N., Haga, A., Naba, N., Shiraiwa, K., Kusakabe, Y., Hashimoto, K., Funasaka, T., Nagase, H., Raz, A., and Nakamura, K. T. (2006) Crystal structures of mouse autocrine motility factor in complex with carbohydrate phosphate inhibitors provide insight into structure-activity relationship of the inhibitors, *J. Mol. Biol. 356*, 312-324.
10. Whittingham, J. L., Edwards, D. J., Antson, A. A., Clarkson, J. M., and Dodson, G. G. (1998) Interactions of phenol and m-cresol in the insulin hexamer, and their effect on the association properties of B28 pro --> Asp insulin analogues, *Biochemistry 37*, 11516-11523.
11. McPhalen, C. A., Vincent, M. G., and Jansonius, J. N. (1992) X-ray structure refinement and comparison of three forms of mitochondrial aspartate aminotransferase, *J. Mol. Biol. 225*, 495-517.
12. Kim, H. K., Liu, J. W., Carr, P. D., and Ollis, D. L. (2005) Following directed evolution with crystallography: structural changes observed in changing the substrate specificity of dienelactone hydrolase, *Acta Crystallogr. D Biol. Crystallogr. 61*, 920-931.
13. Raag, R., Swanson, B. A., Poulos, T. L., and Ortiz de Montellano, P. R. (1990) Formation, crystal structure, and rearrangement of a cytochrome P-450cam iron-phenyl complex, *Biochemistry 29*, 8119-8126.

14. Johnson, S. J., and Beese, L. S. (2004) Structures of mismatch replication errors observed in a DNA polymerase, *Cell 116*, 803-816.
15. Turnbull, W. B., and Daranas, A. H. (2003) On the value of c: can low affinity systems be studied by isothermal titration calorimetry?, *J. Am. Chem. Soc. 125*, 14859-14866.
16. Kadam, R. U., Bergmann, M., Hurley, M., Garg, D., Cacciarini, M., Swiderska, M. A., Nativi, C., Sattler, M., Smyth, A. R., Williams, P., Camara, M., Stocker, A., Darbre, T., and Reymond, J. L. (2011) A glycopeptide dendrimer inhibitor of the galactose-specific lectin LecA and of Pseudomonas aeruginosa biofilms, *Angew. Chem., Int. Ed. 50*, 10631-10635.
17. Kabsch, W. (2010) XDS, *Acta Crystallogr D Biol Crystallogr 66*, 125-132.
18. McCoy, A. J., Grosse-Kunstleve, R. W., Adams, P. D., Winn, M. D., Storoni, L. C., and Read, R. J. (2007) Phaser crystallographic software, *J Appl Crystallogr 40*, 658-674.
19. Perrakis, A., Morris, R., and Lamzin, V. S. (1999) Automated protein model building combined with iterative structure refinement, *Nat Struct Biol 6*, 458-463.
20. Adams, P. D., Afonine, P. V., Bunkoczi, G., Chen, V. B., Davis, I. W., Echols, N., Headd, J. J., Hung, L. W., Kapral, G. J., Grosse-Kunstleve, R. W., McCoy, A. J., Moriarty, N. W., Oeffner, R., Read, R. J., Richardson, D. C., Richardson, J. S., Terwilliger, T. C., and Zwart, P. H. (2010) PHENIX: a comprehensive Python-based system for macromolecular structure solution, *Acta Crystallogr D Biol Crystallogr 66*, 213-221.
21. Emsley, P., and Cowtan, K. (2004) Coot: model-building tools for molecular graphics, *Acta Crystallogr D Biol Crystallogr 60*, 2126-2132.
22. Jorgensen, W. L., Maxwell, D. S., and Tirado-Rives, J. (1996) Development and Testing of the OPLS All-Atom Force Field on Conformational Energetics and Properties of Organic Liquids, *J. Am. Chem. Soc 45*, 11225–11236.
23. Friesner, R. A., Banks, J. L., Murphy, R. B., Halgren, T. A., Klicic, J. J., Mainz, D. T., Repasky, M. P., Knoll, E. H., Shelley, M., Perry, J. K., Shaw, D. E., Francis, P., and Shenkin, P. S. (2004) Glide: a new approach for rapid, accurate docking and scoring. 1. Method and assessment of docking accuracy, *J Med Chem 47*, 1739-1749.
24. Halgren, T. A., Murphy, R. B., Friesner, R. A., Beard, H. S., Frye, L. L., Pollard, W. T., and Banks, J. L. (2004) Glide: a new approach for rapid, accurate docking and scoring. 2. Enrichment factors in database screening, *J Med Chem 47*, 1750-1759.
25. Hamodrakas, S. J., Kanellopoulos, P. N., Pavlou, K., and Tucker, P. A. (1997) The crystal structure of the complex of concanavalin A with 4'-methylumbelliferyl-alpha-D-glucopyranoside, *J Struct Biol 118*, 23-30.
26. Kanellopoulos, P. N., Pavlou, K., Perrakis, A., Agianian, B., Vorgias, C. E., Mavrommatis, C., Soufi, M., Tucker, P. A., and Hamodrakas, S. J. (1996) The crystal structure of the complexes of concanavalin A with 4'-nitrophenyl-alpha-D-mannopyranoside and 4'-nitrophenyl-alpha-D-glucopyranoside, *J Struct Biol 116*, 345-355.
27. Amaya, M. F., Watts, A. G., Damager, I., Wehenkel, A., Nguyen, T., Buschiazzo, A., Paris, G., Frasch, A. C., Withers, S. G., and Alzari, P. M. (2004) Structural insights into the catalytic mechanism of Trypanosoma cruzi trans-sialidase, *Structure 12*, 775-784.
28. Huang, J., Xu, Z., Wang, D., Ogata, C. M., Palczewski, K., Lee, X., and Young, N. M. (2010) Characterization of the secondary binding sites of Maclura pomifera agglutinin by glycan array and crystallographic analyses, *Glycobiology 20*, 1643-1653.

29. Zaccai, N. R., Maenaka, K., Maenaka, T., Crocker, P. R., Brossmer, R., Kelm, S., and Jones, E. Y. (2003) Structure-guided design of sialic acid-based Siglec inhibitors and crystallographic analysis in complex with sialoadhesin, *Structure 11*, 557-567.
30. Rangel, T. B., Rocha, B. A., Bezerra, G. A., Assreuy, A. M., Pires Ade, F., do Nascimento, A. S., Bezerra, M. J., do Nascimento, K. S., Nagano, C. S., Sampaio, A. H., Gruber, K., Delatorre, P., Fernandes, P. M., and Cavada, B. S. (2012) Crystal structure of a pro-inflammatory lectin from the seeds of Dioclea wilsonii Standl, *Biochimie 94*, 525-532.
31. Collins, P. M., Oberg, C. T., Leffler, H., Nilsson, U. J., and Blanchard, H. (2012) Taloside inhibitors of galectin-1 and galectin-3, *Chem Biol Drug Des 79*, 339-346.
32. Vollan, V. B., Hough, E., and Karlsen, S. (1999) Structural studies on the binding of 4-methylumbelliferone glycosides of chitin to rainbow trout lysozyme, *Acta Crystallogr D Biol Crystallogr 55*, 60-66.
33. Oberg, C. T., Blanchard, H., Leffler, H., and Nilsson, U. J. (2008) Protein subtype-targeting through ligand epimerization: talose-selectivity of galectin-4 and galectin-8, *Bioorg Med Chem Lett 18*, 3691-3694.
34. Wang, X. G., Olsen, L. R., and Roderick, S. L. (2002) Structure of the lac operon galactoside acetyltransferase, *Structure 10*, 581-588.
35. Han, Z., Pinkner, J. S., Ford, B., Obermann, R., Nolan, W., Wildman, S. A., Hobbs, D., Ellenberger, T., Cusumano, C. K., Hultgren, S. J., and Janetka, J. W. (2010) Structure-based drug design and optimization of mannoside bacterial FimH antagonists, *J Med Chem 53*, 4779-4792.
36. Transue, T. R., Smith, A. K., Mo, H., Goldstein, I. J., and Saper, M. A. (1997) Structure of benzyl T-antigen disaccharide bound to Amaranthus caudatus agglutinin, *Nat Struct Biol 4*, 779-783.